Available online at www.eccomasproceedia.org
Eccomas Proceedia COMPDYN (2017) 4881-4896

ECCOMAS
Proceedia

COMPDYN 2017
6th ECCOMAS Thematic Conference on
Computational Methods in Structural Dynamics and Earthquake Engineering
M. Papadrakakis, M. Fragiadakis (eds.)
Rhodes Island, Greece, 15–17 June 2017

TOOL FOR SHEAR ANALYSIS OF PRESTRESSED STEEL FIBER CONCRETE BEAMS

P. R. Tadepalli[1], Liang Lu[2], Y. L. Mo[1], and T. T. C. Hsu[1]

[1] Department of Civil and Environmental Engineering, University of Houston, Houston, Texas, USA
e-mail: {tvvssprao, ymo, thsu}@uh.edu

[2] College of Civil Engineering, Tongji University, Shanghai, China
95010@tongji.edu.cn

Keywords: Simulation of Concrete Structure, Prestressed Steel Fiber Concrete, OpenSees, Constitutive Law, Shear.

Abstract. *Prestressed steel fiber concrete beams have been employed in bridge engineering because the conventional shear reinforcement can be replaced by steel fibers, which can reduce the construction labor and provide greater shear strength and ductility than those of conventional prestressed concrete beams. The shear strengths of elements in webs depend strongly on the softening of concrete struts in the principal compression direction due to the principal tension in the perpendicular direction. By studying the shear behavior of isolated web elements, this softening phenomenon has been clarified for monotonic loading in the Softened Membrane Model (SMM) for reinforced concrete. Recently, SMM was extended to prestressed steel fiber concrete. In the present paper, a Finite Element program (Called Simulation of Concrete Structures, SCS) is developed for analysis of shear-critical prestressed steel fiber concrete structures by implementing constitutive laws of prestressed steel fiber concrete into an object-oriented software framework called "Open System for Earthquake Engineering Simulation (OpenSees)" originally developed at the University of California, Berkeley. The new material modules have been integrated with the existing material modules in OpenSees. SCS thus developed has been used for predicting the shear behavior of the prestressed steel fiber concrete I-beams. The analysis could well predict the entire shear behavior of the beams including the initial stiffness, post-cracking stiffness, yield point, and ultimate load for both web shear and flexure shear failure modes. This new tool gives engineers greatly improved simulation capabilities.*

Peer-review under responsibility of the organizing committee of COMPDYN 2017.
doi: 10.7712/120117.5769.18324

1 INTRODUCTION

In conventional prestressed concrete beams, longitudinal prestressed tendons serve to resist bending moment and transverse mild steel stirrups are used to carry shear forces. Producing and placing stirrups, however, requires costly labor and time. To overcome these difficulties, it is proposed to replace the stirrups in prestressed concrete beams with steel fibers. This replacement concept was shown to be feasible in a recently completed project [1].

In addition to experimental work, a finite element analysis tool needs to be developed to better understand the shear behavior of prestressed steel fiber concrete beams. The tool was developed by implementing constitutive models of prestressed steel fiber concrete in OpenSees [2], which stands for Open System for Earthquake Engineering Simulation. It is an object-oriented software framework for simulation applications in earthquake engineering using finite element methods. It is comprised of a set of modules to perform creation of the finite element model, specification of an analysis procedure, selection of quantities to be monitored during the analysis, and the output of results [2]. The features of OpenSees are described on the OpenSees website (www.opensees.berkeley.edu).

2 FORMULATION OF SOFTENED MEMBRANE MODEL

The Softened Membrane Model for Prestressed Steel Fiber Concrete (SMM-PSFC) was developed to predict the behavior of prestressed steel fiber concrete elements under monotonic loading [3]. SMM-PSFC consisted of the equilibrium and compatibility equations along with the constitutive models of materials. However, SMM-PSFC contains the uniaxial constitutive models of materials under monotonic loading only. The details of SMM-PSFC can be found in [1]. The following describes the formulation of softened membrane model for the preparation of finite element analysis implementation to be described in the next section.

2.1 Equilibrium and compatibility equations

The in-plane element considered in this model is shown in Figure 1. The element considered is reinforced by two layers of orthogonal grids of mild steel as well as prestressing steel, oriented at a given angle to the principal stress direction. The first reference Cartesian ℓ-t coordinate system represents the longitudinal and transverse steel bar directions. The second reference Cartesian 1-2 coordinate system represents the direction of the principal stresses. For the computational purposes, it is assumed that the steel bars are uniformly distributed in the ℓ- and t-directions, and the membrane element is of uniform thickness. The principal applied stresses acting on the four boundary edges of the element are assumed to be uniformly distributed.

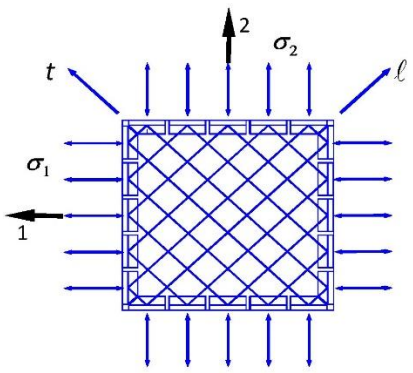

Figure 1: A typical reinforced concrete plane stress element.

The three equilibrium equations, which relate the applied stresses (σ_ℓ, σ_t and $\tau_{\ell t}$) to the internal stresses of concrete (σ_2^c, σ_1^c and τ_{21}^c), mild steel (f_ℓ and f_t), and prestressing steel ($f_{\ell p}$ and f_{tp}) in a membrane element, are given in Equations 1 to 3.

$$\sigma_\ell = \sigma_2^c \cos^2 \alpha_2 + \sigma_1^c \sin^2 \alpha_2 + \tau_{21}^c 2 \sin \alpha_2 \cos \alpha_2 + \rho_\ell f_\ell + \rho_{\ell p} f_{\ell p} \quad (1)$$

$$\sigma_t = \sigma_2^c \sin^2 \alpha_2 + \sigma_1^c \cos^2 \alpha_2 - \tau_{21}^c 2 \sin \alpha_2 \cos \alpha_2 + \rho_t f_t + \rho_{tp} f_{tp} \quad (2)$$

$$\tau_{\ell t} = (-\sigma_2^c + \sigma_1^c) \sin \alpha_2 \cos \alpha_2 + \tau_{21}^c (\cos^2 \alpha_2 - \sin^2 \alpha_2) \quad (3)$$

The three compatibility equations, which represent the relationship between the strains (ε_ℓ, ε_t, and $\gamma_{\ell t}$) in the $\ell - t$ coordinate of the reinforcement and the strains (ε_1, ε_2, and γ_{21}) in the 2-1 coordinate of the principal applied stress, are given in Equation 4 through 6 [4].

$$\varepsilon_\ell = \varepsilon_2 \cos^2 \alpha_2 + \varepsilon_1 \sin^2 \alpha_2 + \frac{\gamma_{21}}{2} 2 \sin \alpha_2 \cos \alpha_2 \quad (4)$$

$$\varepsilon_t = \varepsilon_2 \sin^2 \alpha_2 + \varepsilon_1 \cos^2 \alpha_2 - \frac{\gamma_{21}}{2} 2 \sin \alpha_2 \cos \alpha_2 \quad (5)$$

$$\frac{\gamma_{\ell t}}{2} = (-\varepsilon_2 + \varepsilon_1) \sin \alpha_2 \cos \alpha_2 + \frac{\gamma_{21}}{2} (\cos^2 \alpha_2 - \sin^2 \alpha_2) \quad (6)$$

2.2 Biaxial strains vs. uniaxial strains

To solve the six equilibrium and compatibility equations, given by Equations 1 to 6, the stress-strain relationships of concrete and steel have to be based on the biaxial strains ε_1, ε_2, ε_ℓ and ε_t. Since general laboratory experiments can provide only the uniaxial constitutive relationships of concrete and steel (rather than the biaxial constitutive relationships), the biaxial strains in Equations 4 through 6 must be converted to uniaxial strains before the uniaxial constitutive relationships can be utilized. Thus, a set of four equations has been derived [5] to relate the set of biaxial strains ($\varepsilon_1, \varepsilon_2, \varepsilon_\ell$ and ε_t) to the set of uniaxial strains ($\bar{\varepsilon}_1$, $\bar{\varepsilon}_2$, $\bar{\varepsilon}_\ell$ and $\bar{\varepsilon}_t$) using the Hsu/Zhu ratios (ν_{12}, ν_{21}), as shown in Equations 7 through 10.

$$\bar{\varepsilon}_1 = \frac{1}{1 - \nu_{12}\nu_{21}} \varepsilon_1 + \frac{\nu_{12}}{1 - \nu_{12}\nu_{21}} \varepsilon_2 \quad (7)$$

$$\bar{\varepsilon}_2 = \frac{\nu_{21}}{1 - \nu_{12}\nu_{21}} \varepsilon_1 + \frac{1}{1 - \nu_{12}\nu_{21}} \varepsilon_2 \quad (8)$$

$$\bar{\varepsilon}_\ell = \bar{\varepsilon}_2 \cos^2 \alpha_2 + \bar{\varepsilon}_1 \sin^2 \alpha_2 + \frac{\gamma_{12}}{2} 2 \sin \alpha_2 \cos \alpha_2 \quad (9)$$

$$\bar{\varepsilon}_t = \bar{\varepsilon}_2 \sin^2 \alpha_2 + \bar{\varepsilon}_1 \cos^2 \alpha_2 - \frac{\gamma_{12}}{2} 2 \sin \alpha_2 \cos \alpha_2 \quad (10)$$

Once the uniaxial strains, $\bar{\varepsilon}_1$, $\bar{\varepsilon}_2$, $\bar{\varepsilon}_\ell$ and $\bar{\varepsilon}_t$ are determined, the stresses σ_1^c, σ_2^c, τ_{12}^c, f_ℓ and f_t in Equations 1 through 3 can be calculated using the uniaxial constitutive relationships under cyclic loading.

As mentioned previously, by taking into account the Hsu/Zhu ratios, the SMM was developed to predict the entire behavior (before and after peak point) of reinforced concrete membrane elements under monotonic shear stresses. Two Hsu/Zhu ratios of panels under monotonic shear stresses were presented in detail by [5]. The first ratio ν_{12} (representing the effect of the compression strain in the 2- direction on the tensile strain in the 1- direction) was found to increase with the increase of steel strain and became a constant 1.9 after yielding. The second ratio ν_{21} (representing the effect of the tensile strain in the 1- direction on the compression strain in the 2- direction) was found to be essentially zero throughout the loading history. Equations 11 and 12 gives the value of the Hsu/Zhu ratios of panels under monotonic shear stresses.

$$\nu_{12} = \begin{cases} 0.2 + 850\varepsilon_{sf}, \varepsilon_{sf} \leq \varepsilon_y \\ 1.9, \qquad\quad \varepsilon_{sf} > \varepsilon_y \end{cases} \tag{11}$$

$$\nu_{21} = 0 \tag{12}$$

Where, ε_{sf} is the smeared (average) tensile strain of steel bars in the $\ell -$ and the $t -$ directions, whichever yields first, taking into account the Hsu/Zhu ratios.

2.3 Constitutive relationships of materials

Uniaxial Constitutive Relationships of Prestressed Steel Fiber Concrete - The constitutive model for prestressed SFC along with the factors that will affect prestressed SFC are summarized in this section, including the constitutive relationships of cracked SFC in tension, compression, and shear. The results are plotted in Figure 2. Note that in the discussion the tensile stress is applied in 1-direction and the compressive stress in 2-direction. Development of these constitutive relationships has been reported by [3]. These proposed constitutive relationships of prestressed steel fiber concrete takes into account the effect of presence steel fibers in the concrete.

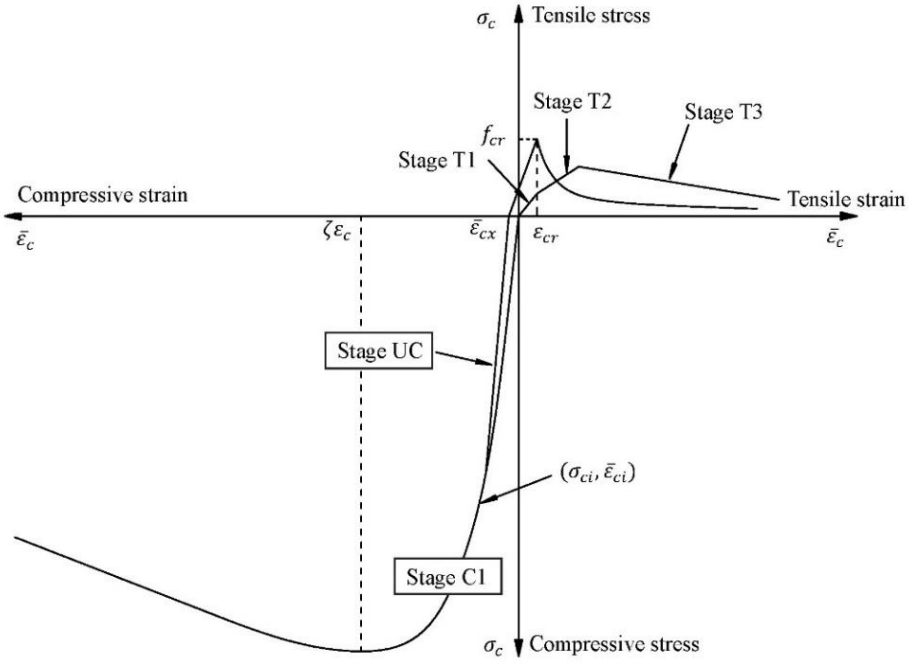

Figure 2: Smeared stress-strain relationships of prestressed steel fiber concrete.

2.3.1 SFC in tension

The relationships of the tensile stress σ_1^c versus the uniaxial tensile strain $\bar{\varepsilon}_1$ of prestressed SFC are given as follows:

Stage UC:

$$\sigma_1^c = E_c'\bar{\varepsilon}_1 + \sigma_{ci},\ \bar{\varepsilon}_1 \le \left(\bar{\varepsilon}_{cx} - \bar{\varepsilon}_{ci}\right) \tag{13a}$$

Stage T1:

$$\sigma_1^c = E_c''(\bar{\varepsilon}_1 + \bar{\varepsilon}_{ci}),\ \left(\bar{\varepsilon}_{cx} - \bar{\varepsilon}_{ci}\right) < \bar{\varepsilon}_1 \le \left(\varepsilon_{cy} - \bar{\varepsilon}_{ci}\right) \tag{13b}$$

Stage T2:

$$\sigma_1^c = E_c'''(\bar{\varepsilon}_1 + \bar{\varepsilon}_{ci}),\ \left(\bar{\varepsilon}_{cy} - \bar{\varepsilon}_{ci}\right) < \bar{\varepsilon}_1 \le \left(\varepsilon_{cult} - \bar{\varepsilon}_{ci}\right) \tag{13c}$$

Stage T3:

$$\sigma_1^c = E^{IV}{}_c(\bar{\varepsilon}_1 + \bar{\varepsilon}_{ci}),\ \bar{\varepsilon}_1 > \left(\varepsilon_{cult} - \bar{\varepsilon}_{ci}\right) \tag{13d}$$

where,

E_c' = decompression modulus of concrete, taken as $\dfrac{2f_c'}{\varepsilon_0}$

$\bar{\varepsilon}_{ci}$ = initial strain in concrete due to prestress

σ_{ci} = initial stress in SFC

$\bar{\varepsilon}_{cx}$ = extra strain in concrete after decompression, calculated by $\bar{\varepsilon}_{ci} - \dfrac{\sigma_{ci}}{E_c'}$

$\varepsilon_{c\max}$ = SFC maximum strain taken as 0.04-ε_{pi}, where, ε_{pi}= initial uniaxial strain of pre-stressing tendons

ε_{cult} = SFC ultimate strain taken as 0.01-ε_{pi}

f_{cult} = SFC ultimate stress strain, taken as $(0.2FF + 12\rho_l)\sqrt{f_c'}$, where: *FF*=fiber factor, ρ_l=longitudinal steel ratio

ε_{cy} = SFC yield strain taken as 0.0005,

f_{cy} = SFC effective "yield" stress for Proportional Loading, taken as $0.4 * FF * CF\sqrt{f_c'}$, (f_c' and $\sqrt{f_c'}$ are in MPa), *CF*=1 for SFC tensile volume confined (sandwiched) by two or more tendons, or *CF*=½ for SFC tensile volume unconfined by tendons

E_c'' = modulus of SFC taken as $\dfrac{f_{cy}}{\varepsilon_{cy} - \bar{\varepsilon}_{cx}}$

E_c''' = modulus of SFC taken as $\dfrac{f_{cult} - f_{cy}}{\varepsilon_{cult} - \varepsilon_{cy}}$

E_c^{IV} = modulus of SFC taken as $\dfrac{-f_{cult}}{\varepsilon_{\max} - \varepsilon_{cult}}$

2.3.2 SFC in compression

The smeared (average) constitutive relationships of SFC compressive stress σ_2^c and the uni-axial compressive strain $\bar{\varepsilon}_2$ are given as follows:

$$\sigma_2^c = \zeta f_c' \left[2\left(\frac{\bar{\varepsilon}_2}{\zeta\varepsilon_0}\right) - \left(\frac{\bar{\varepsilon}_2}{\zeta\varepsilon_0}\right)^2 \right], \frac{\bar{\varepsilon}_2}{\zeta\varepsilon_0} \le 1 \tag{14a}$$

$$\text{or } \sigma_2^c = \zeta f_c' \left[1 - \left(\frac{\bar{\varepsilon}_2/\zeta\varepsilon_0 - 1}{4/\zeta - 1}\right)^2 \right], \frac{\bar{\varepsilon}_2}{\zeta\varepsilon_0} > 1 \tag{14b}$$

Where ζ is the softening coefficient, can be determined as follows:

$$\zeta_\sigma = f(f_c')f(\bar{\varepsilon}_1)f(\beta)W_p Wf \le 0.9, \tag{15}$$

where

$$f(f_c') = \frac{5.8}{\sqrt{f_c'}} \le 0.9 \ (f_c' \text{ in MPa}), \tag{16}$$

$$f(\bar{\varepsilon}_1) = \frac{1}{\sqrt{1 + 400\bar{\varepsilon}_1}}, \tag{17}$$

$$f(\beta) = 1 - \frac{|\beta|}{24^\circ}, \ \beta = \frac{1}{2}\tan^{-1}\left[\frac{\gamma_{21}}{(\varepsilon_2 - \varepsilon_1)}\right] \tag{18}$$

$$W_p = 1.15 + \frac{|\beta|(0.09|\beta| - 1)}{6}, \tag{19}$$

and

$$Wf = 1 + 0.2FF \tag{20}$$

2.3.3 SFC in shear

The rational equation relating the shear stress of concrete (τ_{12}^c) and the shear strain (γ_{12}) in the 1-2 coordinate system is given by [6, 7] and shown in Equation 21.

$$\tau_{12}^c = \frac{\sigma_1^c - \sigma_2^c}{2(\varepsilon_1 - \varepsilon_2)}\gamma_{12} \tag{21}$$

where σ_1^c and σ_2^c are the smeared (average) concrete stresses and ε_1 and ε_2 are the biaxial smeared strains in the 1- and 2- directions of the principal applied stresses, respectively.

2.3.4 Prestressing tendons embedded in SFC

The smeared (average) stress-strain relationships of prestressing tendons embedded in SFC are given as follows and is shown in Figure 3:

$$f_{ps} = E_{ps}\bar{\varepsilon}_s', \ \bar{\varepsilon}_s < \frac{0.7f_{pu}}{E_{ps}} \tag{22a}$$

$$\text{or} \quad f_{ps} = \frac{E''_{ps}\bar{\varepsilon}'_s}{\left[1+\left(\frac{E''_{ps}\bar{\varepsilon}'_s}{f'_{pu}}\right)^5\right]^{\frac{1}{5}}}, \ \bar{\varepsilon}_s \geq \frac{0.7f_{pu}}{E_{ps}} \tag{22b}$$

where

E_{ps} = elastic modulus of prestressing tendons, 200GPa

$\bar{\varepsilon}'_s = \bar{\varepsilon}_s + \varepsilon_{dec}$, uniaxial steel bar strain

f_{pu} = ultimate strength of prestressing tendons, 1860MPa

E''_{ps} = modulus of prestressing tendons in plastic area (Eq. 22), 209MPa

f'_{pu} = modified strength of prestressing tendons, 1793MPa

In the above equations, *ps* can be exchanged by ℓp and tp for the longitudinal tendons and the transverse tendons respectively.

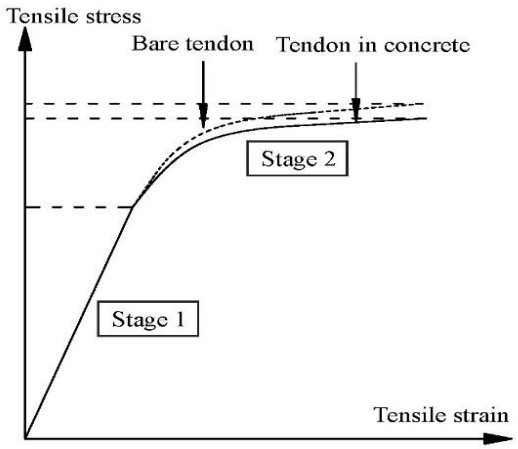

Figure 3: Constitutive relationship of prestressing strands.

2.3.5 Mild Steel Embedded in SFC

The smeared (average) tensile stress-strain relationships of mild steel embedded in concrete in the $\ell - t$ coordinate are the same as those in SMM. They can be expressed as follows and is shown in Figure 4:

Stage 1:

$$f_s = E_s\bar{\varepsilon}_s, \ \bar{\varepsilon}_s \leq \bar{\varepsilon}_n \tag{23}$$

Stage 2:

$$f_s = f_y\left[(1-0.096FF)(0.91-2B)+(0.2FF+1)(0.02+0.25B)\frac{\bar{\varepsilon}_s}{\varepsilon_y}\right], \ \bar{\varepsilon}_s > \bar{\varepsilon}_n \tag{24}$$

Stage 3 (unloading):

$$f_s = f_p - E_s(\bar{\varepsilon}_p - \bar{\varepsilon}_s), \ \bar{\varepsilon}_s < \bar{\varepsilon}_p \tag{25}$$

where

$$\bar{\varepsilon}_n = \varepsilon_y(0.93 - 2B) \tag{26a}$$

$$B = \frac{1}{\rho}\left(\frac{f_{cr}}{f_y}\right)^{1.5} \tag{26b}$$

ε_{cr} = 0.00008, concrete cracking strain

$f_{cr} = 0.31\sqrt{f_c'}$ (f_c' and $\sqrt{f_c'}$ are in *MPa*), concrete cracking stress

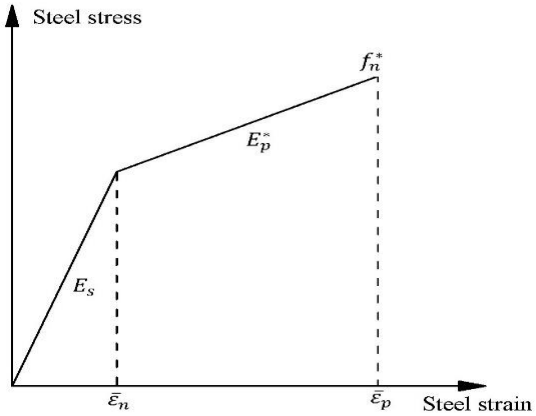

Figure 4: Stress-strain relationship of reinforcing steel using two-straight line expression.

3 IMPLEMENTATION OF SOFTENED MEMBRANE MODEL

Once the softened membrane model is developed, it needs to be implemented in a finite element analysis program, such as OpenSees. Under the OpenSees framework, each finite element analysis consists of four main types of objects: *ModelBuilder* object, *Domain* object, *Analysis* object, and *Recorder* object, as shown in Figure 5.

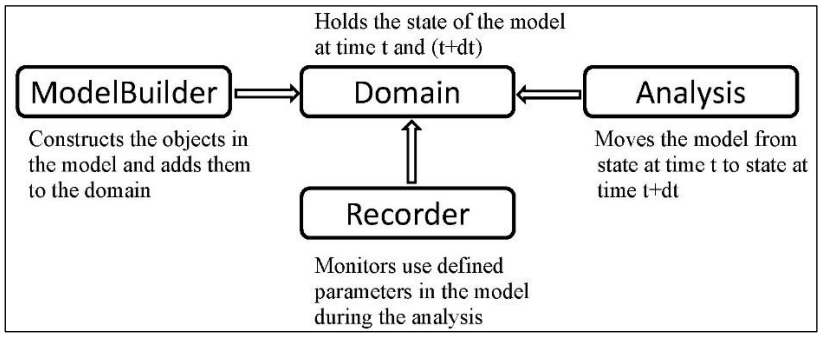

Figure 5: Principal objects in OpenSees [2].

The *ModelBuilder* object constructs the nodes and masses on the nodes, creates the elements and materials of the elements, defines the loads acting on the nodes and the elements, and defines the constraints acting on the nodes. The *ModelBuilder* is responsible for building the objects in the model such as *Node*, *Mass*, *Material*, *Element*, *LoadPattern*, *Constraint*, etc. and adding them to the *Domain*.

After the objects are created by the *ModelBuilder* object, they are stored in the *Domain* object. The *Domain* object also provides access of *Analysis* and *Recorder* objects to the objects in the *Domain* and holds the state of the model during the analysis procedure.

The *Analysis* object is responsible for performing static or dynamic analysis on the model. The *Analysis* object includes object such as *ConstraintHandler*, *Numberer*, *AnalysisModel*, *SolutionAlgorithm*, *Integrator*, and *SystemOfEquation*. These objects define how the analysis is performed. The *ConstraintHandler* object defines the relationships between the degrees of freedom (DOF) of the nodes and determines the constraint equation in the analysis. The *Numberer* object is used to construct the *DOF_Numberer* object, which determines the mapping between equation numbers and degrees-of-freedom. The *AnalysisModel* object comprises many *FE_Element* objects and *DOF_Group* objects. The *SolutionAlgorithm* object defines the solution algorithm that is used to solve the nonlinear equation.

Currently, the *SolutionAlgorithm* objects in OpenSees includes many methods such as Linear, Newton-Raphson, Modified Newton-Raphson, Newton-Raphson with line search, Newton-Raphson with acceleration and other algorithms. The *Integrator* object determines the predictive step and corrective step during the time t+dt in the analysis and specify the tangent matrix and residual vector at any iteration. The type of *Integrator* is different for static analysis and dynamic analysis. The *Integrator* objects for static analysis include load control, displacement control and arc-length control. The *Integrator* objects for dynamic analysis include Newmark method, Wilson-θ method, Hilbert-Hughes-Taylor method and other methods. The System of Equation objects are used to store and solve the system of equations in the analysis. The *Recorder* object is used to monitor the state of *Domain* components during an analysis, and write the state to a file or to a database.

Under this framework, if a new type of element or new material is to be introduced, a new corresponding class of objects can be added to the OpenSees according to the designated specification of the framework without changing the existing code. This is because the interface, which is defined in the core components, is minimal to make adding new component classes easier but large enough to ensure all that is required can be accommodated [2].

The OpenSees is not able to perform nonlinear finite element analysis on reinforced concrete membrane structures such as panels and shear walls because there is no membrane model for reinforced concrete. Also, the uniaxial material models of concrete and steel in OpenSees are too simple, and more sophisticated models need to be created. For example, the concrete model *Concrete01* in OpenSees does not consider the stress of concrete in tension and the softening effect in compression due to the biaxial tensile strain in the perpendicular direction. The steel model *Steel01* does not take into account the Bauschinger effect in the unloading and reloading paths. Therefore, the new finite element models of reinforced concrete plane stress material could be implemented into OpenSees for performing analysis on reinforced concrete membrane structures.

Uniaxial material class, *ConcreteR01* is created and implemented into OpenSees in addition to *TendonL01* [8] and *SteelZ01* [9], which were implemented previously. An object of *ConcreteR01* needs three input parameters: ultimate compressive strength $f_c^{'}$, fiber factor ($FF = V_f \frac{L_f}{D_f}$, product of volume of steel fiber in concrete and aspect ratio of steel fiber) and the compressive strain ε_0 corresponding to $f_c^{'}$. An object of *SteelZ01* needs four input parameters: yield stress, Young's modulus, concrete compressive strength, and steel ratio. The latter two parameters are used to calculate the smeared yield stress and strain of embedded rebars. In addition, the coefficients in *A* and *R* that determine the shapes of unloading and reloading paths are set as two additional input parameters. The default values are defined as 1.9 and 10.0. An object of *TendonL01* needs five input parameters. The first four input parameters are the same as the ones required for *SteelZ01*. The fifth input parameter required is the initial strain in the

prestressing tendons. The additional input parameters, *A* and *R*, to determine the shapes of the unloading and reloading paths are also available with default values of 1.9 and 10.0 respectively.

A 2D material class *PCPlaneStress* is created and implemented into OpenSees by Laskar [8]. The *PCPlaneStress* is a class for reinforced/prestressed concrete plane stress material using CSMM-PC. In *PCPlaneStress*, the material constitutive matrix is evaluated and the stress vector is calculated. An object of *PCPlaneStress* material needs the tags of the created uniaxial concrete, steel, and tendon objects of *ConcreteR01*, *SteelZ01*, *and TendonL01*, the directions of the steel and tendon grids, and the steel and tendon ratio for the steel in each direction. Two uniaxial concrete objects are needed in defining one *PCPlaneStress* object, which represents the concrete in the two principal stresses directions. The steel and tendon orientations are not necessarily in the horizontal and vertical directions, and the user can define the arbitrary angles of the steel and tendons. The steel and tendon directions are not necessarily orthogonal, either. Currently users can define the steel in the prestressed concrete element in up to two directions and the tendons in the prestressed element in another two directions.

The implementation of the *PCPlaneStress* into OpenSees is shown in Figure 6. The Analysis and *Recorder* objects are omitted in this figure. The *PCPlaneStress* is implemented with the *Quadrilateral* element to represent the PC plane stress four node elements. The *PCPlaneStress* is related with *ConcreteR01*, *SteelZ01* and *TendonL01* to determine the tangent material constitutive matrix and calculate the stress of the elements. For each trial displacement increment in the analysis procedure, *PCPlaneStress* will receive the strains of the elements, determine the uniaxial strains of the concrete and steel, and then send the uniaxial strain of concrete and tensile perpendicular strain to the two uniaxial concrete objects. After receiving the uniaxial strain and corresponding tensile strain, the concrete object will calculate the tangent stiffness and stress and then send the values back to the *PCPlaneStress* object. Similarly, *PCPlaneStress* will send the uniaxial strain of the steel to the uniaxial steel object and receive the tangent stiffness and stress from the related uniaxial steel objects. As in the case of steel, *PCPlaneStress* also sends the uniaxial strain of tendon to the uniaxial tendon object. After receiving the uniaxial strain, the tendon object will add the initial strain in the tendon to the received strain and thereafter calculate the tangent stiffness and stress to be sent back to the *PCPlaneStress* object. After receiving the uniaxial stiffness and stress of concrete, steel, and tendons the tangent stiffness matrix will be evaluated and the stress vector calculated. An iterative procedure is defined to obtain the converged material constitutive matrix and stress vector for a given strain vector.

Meanwhile, the displacement control scheme in the OpenSees has been previously modified for an arbitrary displacement path to perform analysis of *RCPlaneStress* structures [9]. The user can define the displacement paths of the degree-of-freedom of the node whose response controls the solution. The displacement increment for each path of the displacement scheme can also be varied. Changing the size of displacement increment makes it possible to overcome some numerical problems in the nonlinear analysis.

In addition, some classes are modified to overcome or bypass the numerical problems occurring in the analysis of nonlinear problems [9]. For example, the analytical models about the convergence check has been modified. Instead of giving one maximum iterative number for all increments, the user can decide different maximum iterative numbers for different paths in the displacement control history. Users can increase the maximum iterative number in the specified path that may have numerical problems. Less iterative numbers in the rest of the displacement paths are defined to save time.

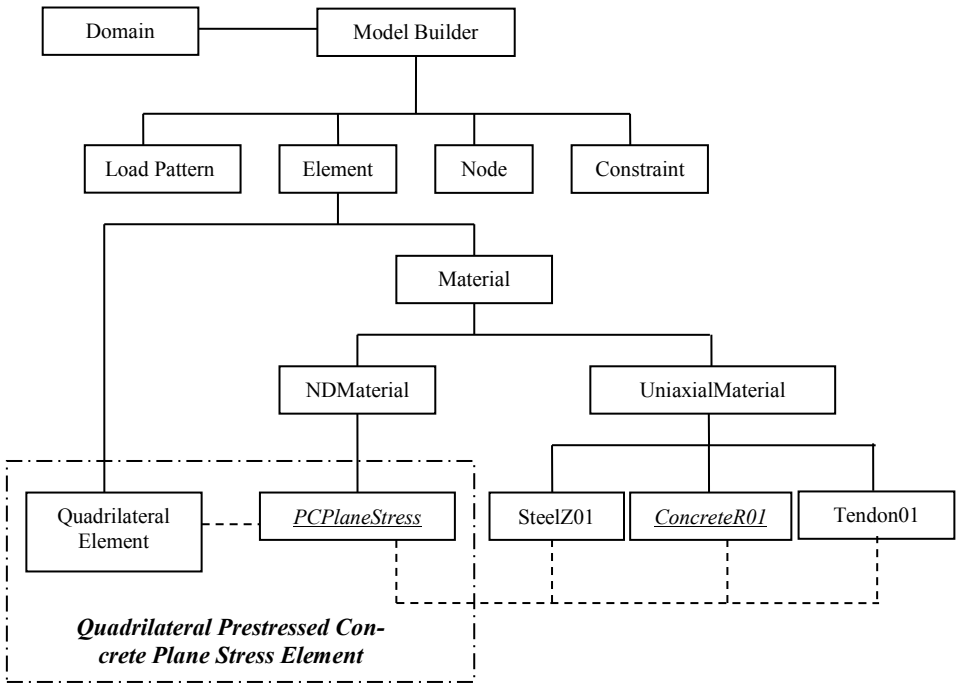

Figure 6: Finite element implementation of CSMM-PC.

4 VALIDATION OF THE DEVELOPED TOOL

To validate the developed tool (called Simulation of Concrete Structures, SCS), the Prestressed Steel Fiber Concrete (PSFC) beams shown in Figure 7 have been selected. Since the PSFC beams were tested under monotonic loads, this validation and applicability of SCS program is only suitable in predicting the behaviour of PSFC structures under monotonic loading. The following describes the analytical details.

4.1 Analytical Model

Various finite element models of the PSFC beams were developed to analyze the beams using SCS program. The two (top and bottom) flanges of the beams, which were designed to resist applied bending moments, were modeled as *NonlinearBeamColumn* elements with fiber sections. The beam web, designed to resist the applied shear force, was represented by *PCPlaneStress Quadrilateral* elements. The details of the finite element models of PSFC beams are described later in this paper. In the finite element model of the PSFC beams the prestressing loads acting on the beam were applied as nodal forces adjacent to the ends of the beams. In case of flexure-shear critical beams, a reduction of 20% in the initial prestressing force is considered to account for prestress loss. An incremental load-control was used for the prestressing loads at the beginning of an analysis in the model. Thereafter, the prestressing loads were kept constant and monotonic vertical loads were applied on the top flange of the beam using a predetermined displacement-control scheme.

All the concentrated loads applied on the beam in the model acted at nodes. The effect of bearing plates, which were actually used in the load-test to apply vertical loads on the beam, was ignored for simplicity. The loads were distributed among three nodes adjacent to the location of the applied load. The analysis yielded similar results in the cases when (a) larger load was applied at the node corresponding to the actual loading point and lower loads were applied at the two adjacent nodes and (b) loads were distributed equally among the three nodes. Hence, the concentrated vertical loads on the beams were modeled at a node corresponding to the actual

loading point and two adjacent nodes. The results of beam analysis i.e. nodal displacement and corresponding vertical forces, were computed at every displacement step that had numerically converged. Additionally, the stresses and strains in the beam elements were also calculated by the program [8].

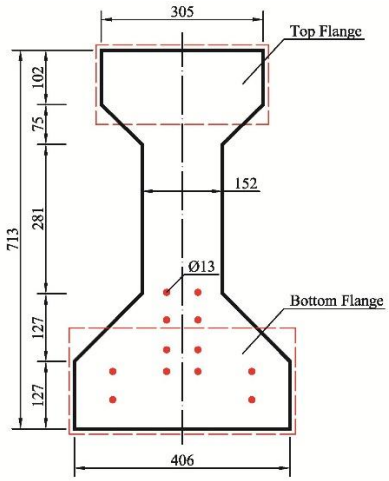

Figure 7: Cross sections of I-beam.

4.2 Finite element model of PSFC beams

Each of the PSFC I-beams was modeled using the finite element mesh, as shown in Figures 8 and 9. The top and bottom flanges in the beams were each divided into sixteen and fifteen *NonlinearBeamColumn* elements in the case of web-shear and flexure-shear failure modes, respectively. The bulb-shaped top and bottom flanges in beam's cross-section were modeled using rectangular *NonlinearBeamColumn* elements with equivalent area. Each *NonlinearBeamColumn* element was defined with two control sections. Each section representing the top flange was discretized into forty fibers of concrete. The configuration of the section discretization of the top flange is shown in Figure 10(a). Similarly, each section representing the bottom flange was discretized into forty fibers of concrete and two fibers of tendons. The configuration of the section discretization of the bottom flange is shown in Figure 10(b).

Two of the twelve tendons in the specimens were provided in the *NonlinearBeamColumn* elements representing the bottom flange of the specimens. The remaining tendons were provided in the quadrilateral elements used to represent the webs of these specimens. The initial strains in the tendons in the web were applied using the *TendonL01* constitutive module. *Concrete01*and *Steel02* material modules were used to define the concrete and steel fibers materials in the cross section, respectively.

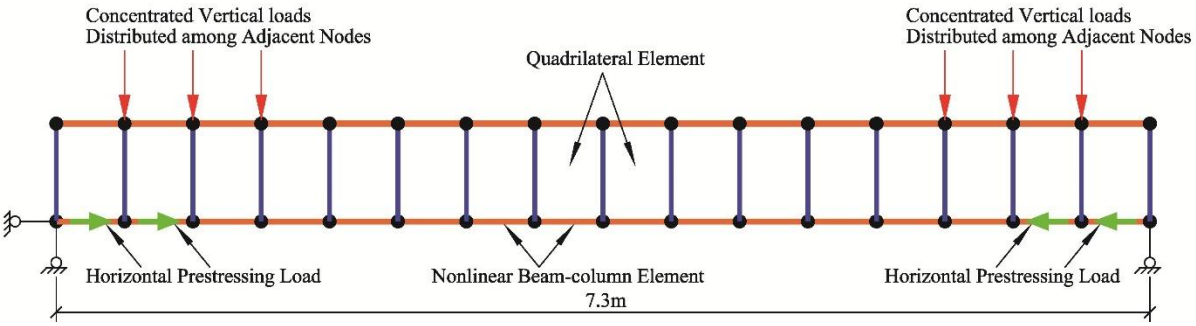

Figure 8: Finite element model of PSFC I-beams tested under web-shear.

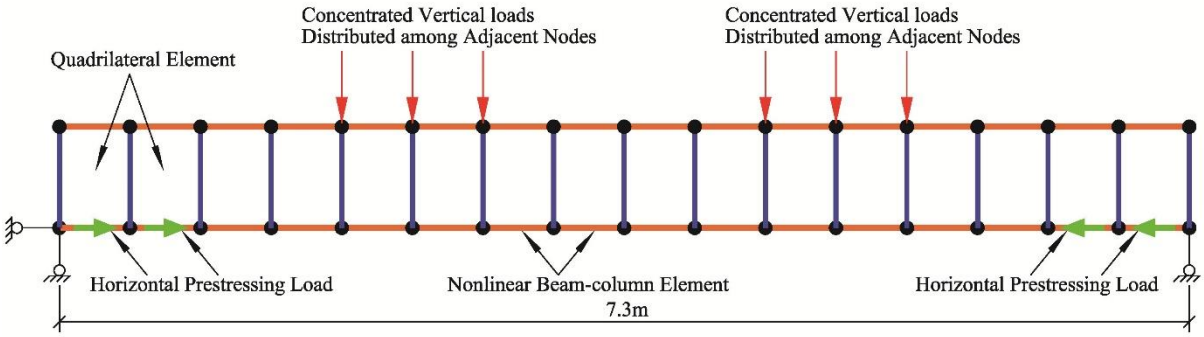

Figure 9: Finite element model of PSFC I-beams tested under flexural-shear.

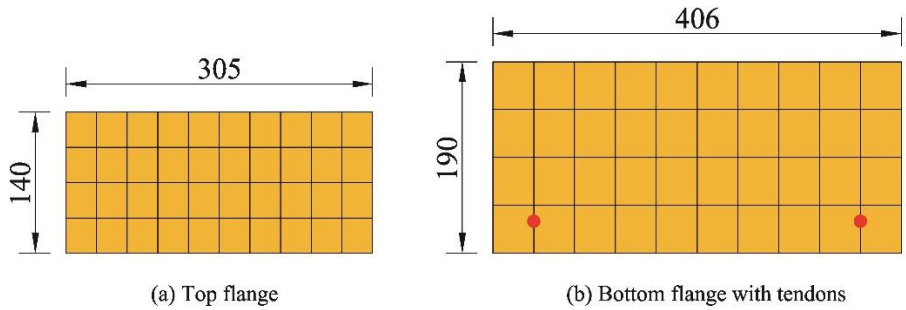

Figure 10: Cross-section discretization for PSFC I-beams governed by web-shear.

The *Concrete01* module used herein was a uniaxial material module of concrete previously created in OpenSees following the modified Kent and Park model [10]. The *steel02* module used in this program was a uniaxial Menegotto-Pinto steel material object with isotropic strain hardening [11]. This object also allowed user to enter the initial strain in the steel, which is useful in modeling the prestressing strands.

The web regions of the beams have been modeled by sixteen and fifteen *PCPlaneStress quadrilateral* elements in case of web shear and flexural shear, respectively. The tendon orientation in the elements was defined in the horizontal direction. The steel ratio in the vertical direction was taken as a very small number to avoid numerical problems during the analysis. The tendon ratio in the horizontal direction was determined based on the area of ten prestressing tendons smeared over the entire cross section of these specimens. *ConcreteR01* and *TendonL01* were used to create the uniaxial material models of concrete and tendons in the *PCPlaneStress* material, respectively. The constant *k* used in *ConcreteR01* was to impose an upper limit to the initial stress-strain relationship of concrete in compression and which reduced the initial slope of the concrete stress-strain curve to less than $\frac{2f_c'}{\varepsilon_0}$. This initial slope of concrete stress-strain curve was taken as 1.5 for the analysis of all the beams tested.

4.3 Comparison of analytical and experimental results

4.3.1 Web-shear failure

The measured and calculated load-displacement curves for all PSFC I-beams tested in web-shear failure mode are shown in Figures 11 to 14. It can be seen that the analyses predict reasonably well the load-displacement characteristics of the beams including initial stiffness, post-cracking stiffness, yield displacement, and ultimate strengths. The general trend observed in the beam (R1 to R4) tests, i.e. increase in load carrying capacity of beams with increase in fiber–factor, was accurately predicted by the analysis program. Figures 11 to 14 also justifies the use

of the constant k =1.4 (close to k = 1.5 assumed initially in the analysis) to make the initial slope of the concrete compressive stress-strain curve lower than $\frac{2f_c'}{\varepsilon_0}$.

Unlike Beams R1, R2 and R3 the prediction of the post-cracking stiffness of Beam R4 did not match well with the experimental results. This is due to the fact that while testing Beam R4, the Data Acquisition System (DAS) got some problem in the electronic part and recorded invalid values and stopped after some time. After resolving the problem with DAS, the test has been restarted. This invalid data is the reason for the lower cracking value and post cracking stiffness observed during the testing of the beam than those obtained from the analysis.

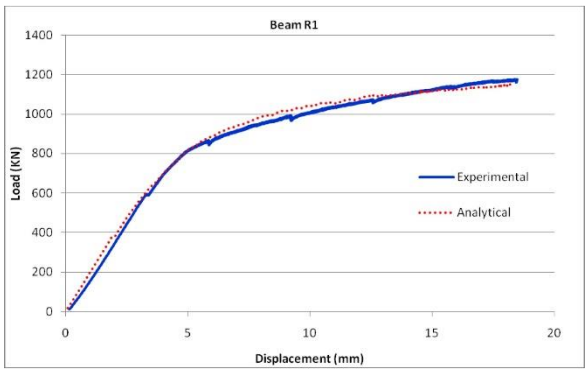

Figure 11: Comparison of experimental and analytical results of beam R1.

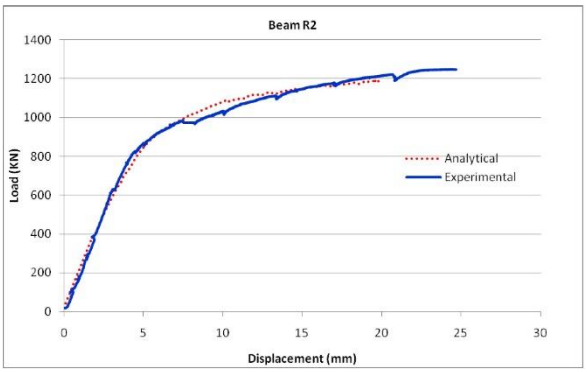

Figure 12: Comparison of experimental and analytical results of beam R2.

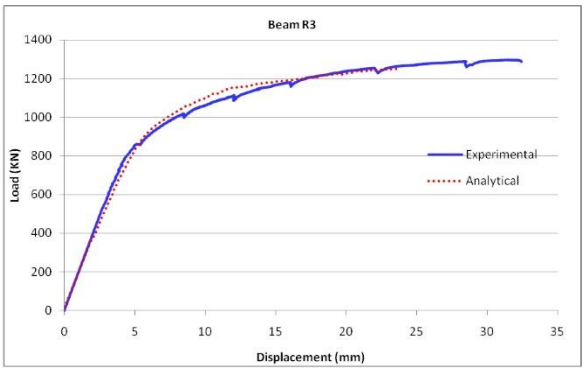

Figure 13: Comparison of experimental and analytical results of beam R3.

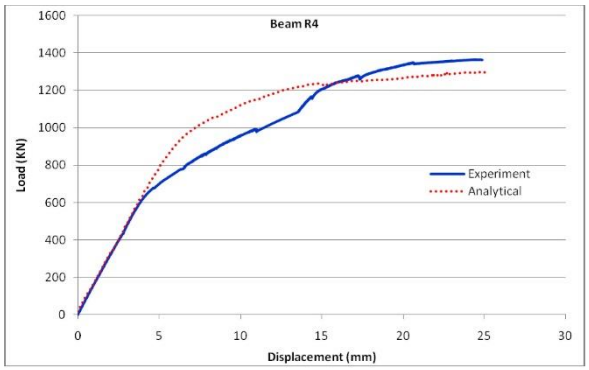

Figure 14: Comparison of experimental and analytical results of beam R4.

4.3.2 Flexure-shear failure

The measured and calculated load-deformation curves for all beams with flexure-shear failure are shown in Figures 15 and 16. Compared with the experimental results, the analyses predicted the load versus deformation characteristics of the specimens including initial stiffness, post-cracking stiffness, yield displacement, and ultimate strength. The analysis could well predict the lower load carrying capacity of beams tested under flexural shear in comparison to the beams tested under web shear failure having same amount of steel fibers. The higher ductility observed in the behavior of beams under flexural-shear failure, than all the web shear specimens was also well predicted in the analysis. Like the beams tested under web shear, Figures 15 and 16 also justifies the use of the constant k = 1.4 to make the initial slope of the compressive stress strain curve of concrete lower than $\frac{2f_c'}{\varepsilon_0}$.

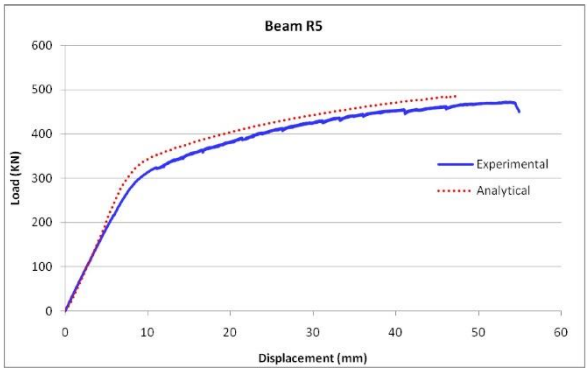

Figure 15: Comparison of experimental and analytical results of beam R5.

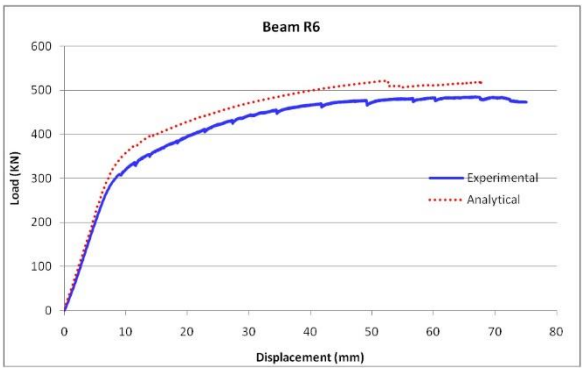

Figure 16: Comparison of experimental and analytical results of beam R6.

5 CONCLUSIONS

The constitutive models of PSFC was previously established. Using the established constitutive models, a softened membrane model for PSFC is formulated, and both the constitutive models for materials and softened membrane model for elements are implemented in a finite element program framework (OpenSees) to develop an analytical tool for shear analysis of the PSFC beams. Using this finite element analysis tool, the load-deflection curves of all the PSFC I-beams are simulated with acceptable accuracy.

ACKNOWLEDGMENTS

The authors would like to express their gratitude to the following sponsors for this project. They are Texas Department of Transportation, Texas, USA, and the National Natural Science Foundation of China (Grant No. 51678453). The materials presented are the research findings by the authors, and are not necessarily expressed for the funding agencies' opinion.

REFERENCES

[1] P.R. Tadepalli, N. Hoffman, T.T.C. Hsu, Y.L. Mo, *Steel Fiber Replacement of Mild Steel in Prestressed Concrete Beams.* Texas Department of Transportation Report 0-5255-2, 2010.

[2] G.L. Fenves, Annual Workshop on Open System for Earthquake Engineering Simulation. *Pacific Earthquake Engineering Research Center, UC Berkeley, http://opensees.berkeley.edu/*, 2008.

[3] N. Hoffman, Constitutive Relationships of Prestressed Steel Fiber Concrete Membrane Elements. *PhD. Dissertation, Department of Civil and Environmental Engineering, University of Houston*, USA, 2010.

[4] X.B. Pang, T.T.C. Hsu, Fixed Angle Softened Truss Model for Reinforced Concrete. *ACI Structural Journal*, **93**, 197-207, 1996.

[5] R.R.H. Zhu, T.T.C. Hsu, Poisson Effect in Reinforced Concrete Membrane Elements. *ACI Structural Journal*, **99**, 631-640, 2002.

[6] T.T.C. Hsu, Y.L. Mo, *Unified Theory of Concrete Structures*, John Wiley and Sons, 2010.

[7] R.R.H. Zhu, T.T.C. Hsu, J.Y. Lee, Rational Shear Modulus for Smeared-Crack Analysis of Reinforced Concrete. *ACI Structural Journal*, **98**, 443-450, 2001.

[8] A. Laskar, Shear Behavior and Design of Prestressed Concrete Members. *PhD. Dissertation, Department of Civil and Environmental Engineering, University of Houston*, USA, 2009.

[9] J.X. Zhong, Model-Based Simulation of Reinforced Concrete Plane Stress Structures. *Ph.D. Dissertation, Department of Civil and Environmental Engineering, University of Houston*, Houston, USA, 2005.

[10] R. Park, M.J.N. Priestley, W.D. Gill, Ductility of Square-Confined Concrete Columns. *Journal of the Structure Division, ASCE,* **108(ST4)**, 929–950, 1982.

[11] R.P. Dhakal, K. Maekawa, Path-dependent Cyclic Stress-Strain Relationship of Reinforcing Bar Including Buckling. *Engineering Structures*, **24**, 1383-1396, 2002.